Quantum Electronics **51** (2) 175–183 (2021)

FIBRE-OPTIC SENSORS

https://doi.org/10.1070/QEL17369

Effect of strong local stretching of sensing fibre on the operation of a phase-sensitive optical time-domain reflectometer

D.M. Bengalskii, D.R. Kharasov, E.A. Fomiryakov, S.P. Nikitin, O.E. Nanii, V.N. Treshchikov

Abstract. **It has been shown experimentally and confirmed by numerical simulation that strong local stretching of sensing fibre distorts the signal detected by a phase-sensitive optical time-domain reflectometer (OTDR) from the fibre section behind the local disturbance region. Comparison of experimental data with theoretical estimates and numerical simulation results leads us to conclude that the physical mechanism underlying the distortion of the OTDR trace is related to the external disturbance-induced variable shift of the optical carrier frequency of probe pulses.**

Keywords: *fibre-optic sensor, distributed sensor, phase-sensitive optical reflectometer, piezoelectric effect, piezoelectric fibre modulator, strong impact on fibre, frequency modulation, correlation.*

1. Introduction

Phase-sensitive optical time-domain reflectometers (ϕOTDRs) have found application as distributed acoustic and temperature sensors for monitoring and protecting extended objects, such as pipelines, railways, motor roads, and others [1–3]. ϕOTDRs typically employ standard single-mode optical fibre as a sensing element [1–3], but to increase their operation range or ensure specialty applications use is made of sensing elements based on fibre combinations or specialised fibres with an increased scattering coefficient [4–9].

ϕOTDRs usually operate in amplitude mode, where the backscattered signal intensity is measured [1]. There are also methods that allow one to turn to phase mode, in which one can analyse phase changes at different points of fibre. The main of such approaches include the use of a dual-pulse configuration [10–12] and an unbalanced Mach–Zehnder interferometer in the receiving part of the ϕOTDR [13].

The sensitivity of ϕOTDRs to external influences depends on the internal noise level, in particular on the stability and reproducibility of test laser output parameters [14]. If the noise in the photoreceiving channel is low, sensitivity over the first few kilometres of the fibre is determined by phase noise and variations in laser frequency. Previous results [15] demonstrate that, in the case of lasers with slow variations in centre frequency (slower than 1 MHz s^{-1}), the signal-to-noise ratio for the photocurrent through a ϕOTDR measured during a time interval of 0.1 s is inversely proportional to the instantaneous Lorentzian width of the laser line.

ϕOTDRs are known to be sensitive to optical frequency shifts. In particular, as shown by Mermelstein et al. [16] changes in the centre frequency of rectangular probe pulses (PPs) lead to changes in the corresponding ϕOTDR traces. Changes in the shape of a ϕOTDR trace can be quantified by the degree of correlation between two ϕOTDR traces to be compared. If the optical frequency shift is $\Delta\nu \ll 1/\tau_p$, where τ_p is the PP duration, the correlation coefficient approaches unity and the shape of the ϕOTDR trace changes little. With increasing $\Delta\nu$, the shape of the ϕOTDR trace becomes more severely distorted, and at $\Delta\nu = 1/\tau_p$ the ϕOTDR traces of the two pulses being compared are completely uncorrelated. Clearly, such large variations in carrier frequency are rarely encountered in practice, but even considerably smaller frequency changes during the time interval between consecutive ϕOTDR traces limit the sensitivity of the ϕOTDR. The effect of laser centre frequency drift on the signal-to-noise ratio in ϕOTDR traces was studied numerically and experimentally by Zhirnov et al. [17]. Zhu et al. [18] proposed a correlation method for laser frequency self-stabilisation.

The possibility of increasing the operation range of ϕOTDRs by raising the PP power is limited by nonlinear effects: modulation instability [19–21], self-phase modulation [20], stimulated Raman scattering (SRS), and stimulated Brillouin scattering (SBS) [20, 22]. At the same time, a distributed Raman (SRS) amplifier [23, 24] or counterpropagating distributed Brillouin (SBS) amplifier [25] allows the operation range of ϕOTDRs to be increased.

Alekseev et al. [26, 27] assessed the accuracy of ϕOTDRs in detecting the signal from a longitudinal acoustic disturbance and showed that it depended on the linearity of their response to the external influence and the nonlinear distortion induced by the random character of multiple-beam interference. Besides, local influences on a portion of a fibre-optic cable were previously thought to affect only the ϕOTDR signal from that portion. However, it follows from the present results that this is so only in the case of relatively weak (in terms of fibre stretching) and slow influences. Relatively strong local disturbances cause interference to the ϕOTDR signal from the fibre beyond the affected region, which may reduce the sensitivity of the reflectometer to external influences in the unaffected region.

Preliminary results show that, in monitoring objects where fibre is subjected to strong external influences, the

D.M. Bengalskii, E.A. Fomiryakov, O.E. Nanii T8 Sensor LLC, Krasnobogatyrskaya ul. 44/1, 107076 Moscow, Russia; Faculty of Physics, Lomonosov Moscow State University, Vorob'evy gory, 119324 Moscow, Russia; e-mail: bengalskiy@t8.ru;
D.R. Kharasov T8 Sensor LLC, Krasnobogatyrskaya ul. 44/1, 107076 Moscow, Russia; Moscow Institute of Physics and Technology (National Research University), Institutskii per. 9, 141701 Dolgoprudnyi, Moscow region, Russia;
S.P. Nikitin, V.N. Treshchikov T8 Sensor LLC, Krasnobogatyrskaya ul. 44/1, 107076 Moscow, Russia

Received 16 May 2020; revision received 10 August 2020
Kvantovaya Elektronika **51** (2) 175–183 (2021)
Translated by O.M. Tsarev

ϕOTDR signal can be distorted. Since this phenomenon is rather widespread, we set the goal to find a quantitative relation between characteristics of an external influence and distortion of a TDR trace and to identify the physical mechanism of the distortion. As previous studies indicated that PP frequency variations caused by frequency drift of a narrowband master oscillator led to distortion of the entire ϕOTDR trace [16, 17], we assumed that the observed effect was also due to frequency variations caused by a strong external influence.

To achieve the goal in question, we carried out an experimental study and numerical simulation of the effect of an external determinate local disturbance on the shape of amplitude and phase ϕOTDR traces. A variable external influence was produced by a piezoelectric fibre transducer (PZT) located in the fibre section being tested. In this configuration, light passed twice through the PZT: as a PP in the forward direction and as backscattered light in the backward direction. The effect of a local disturbance on the shape of ϕOTDR traces was studied at PZT positions such that the contributions of these two distinct physical processes were separated.

2. Schematic of the experimental setup

To experimentally verify the assumption that distortions of ϕOTDR traces are due to frequency variations caused by a strong external influence, we produced an experimental setup that allowed us not only to measure characteristics of amplitude and phase ϕOTDR traces but also to monitor variations in the PP and scattered light frequencies.

A strong determinate local disturbance was produced by a piezoelectric fibre modulator in the form of a fibre section wound onto a piezoelectric element, to which a voltage from an external signal generator (SG) was applied. The phase change of the light, φ_{mod}, at the PZT output is proportional to the fibre elongation ΔL in the PZT, which is in turn proportional to the voltage applied to the piezoelectric element: $\Delta L \propto U$. Thus, U and φ_{mod} are related linearly:

$$\varphi_{\text{mod}}(t) = K(f_{\text{SG}})U(t), \tag{1}$$

where the proportionality coefficient $K(f_{\text{SG}})$ depends on frequency f_{SG} and also on the material and geometry of the piezoelectric element and the way in which the fibre is attached to it.

If a sinusoidal voltage $U(t) = U_0\sin(2\pi f_{\text{SG}}t)$ is applied to the PZT, the phase modulation (1) induced in it leads to a time-dependent shift of the optical carrier frequency:

$$\Delta\omega(t) = \varphi'_{\text{mod}}(t) = \Delta\omega_0\cos(2\pi f_{\text{SG}}t), \tag{2}$$

$$\Delta\omega_0 = K(f_{\text{SG}})\,U_0\,2\pi f_{\text{SG}}. \tag{3}$$

The propagation of a quasi-continuous optical signal of duration comparable to the PP period through the PZT will be accompanied by a sinusoidal frequency modulation described by (2). In particular, the propagation of backscattered (towards the reflectometer) light through the PZT is accompanied by frequency modulation described by relations (2) and (3). The modulation frequency f_{SG} is determined by the PZT modulation frequency, and the amplitude $\Delta\omega_0$ is given by (3).

The propagation of short optical pulses, in particular, PPs from the reflectometer, whose duration is much shorter than the disturbance period ($t_{\text{SG}} = f_{\text{SG}}^{-1}$) is accompanied by a shift of the optical frequency carrier. The variation in frequency shift during a pulse is then small ($\delta\omega_0 \ll \Delta\omega_0$) and can be neglected. Indeed, the maximum shift $\Delta\omega_0$ and the maximum variation in the shift $\delta\omega_0$ of the optical carrier during a PP are related by the simple formula

$$\delta\omega_0(\tau_{\text{p}}) = \Delta\omega_0 2\pi f_{\text{SG}}\tau_{\text{p}}. \tag{4}$$

Since $\tau_{\text{p}} \ll f_{\text{SG}}^{-1}$, we have $\delta\omega_0 \ll \Delta\omega_0$, so the frequency variation during a pulse can be neglected.

In most ϕOTDRs, fibre is probed by short pulses tens to hundreds of nanoseconds in duration, with a repetition rate $f_{\text{p}} \sim 1$ kHz and period $T_{\text{p}} \sim 1$ ms. The PZT-induced shift of the optical carrier frequency of PPs is given by relation (2) at discrete points in time: $t(N) = t_1 + (N-1)T_{\text{p}}$. Substituting the time when the Nth pulse passes through the PZT into (2), we obtain the following relation for the frequency shift of the Nth pulse:

$$\Delta\omega(N) = \omega(t(N)) = \Delta\omega_0\cos[\varphi_1 + 2\pi f_{\text{SG}}(N-1)\,T_{\text{p}}], \tag{5}$$

where φ_1 is the phase of the first pulse when it passes through the PZT. For $f_{\text{SG}} > f_{\text{p}}$, there is a stroboscopic effect, which causes the pulse centre frequency to oscillate not at frequency f_{SG}, in contrast to Eqn (5), but at frequency $f_{\text{mod}} = f_{\text{SG}} - f_{\text{p}}[f_{\text{SG}}/f_{\text{p}} + 0.5]$, equal to the difference between f_{SG} and the nearest multiple of the probe frequency f_{p}, where the square brackets represent the integral part of the number. Note that f_{mod} does not exceed $f_{\text{p}}/2$ and lies in the range from $-f_{\text{p}}/2$ to $f_{\text{p}}/2$. The relation for the frequency shift then takes the form

$$\Delta\omega(N) = \Delta\omega_0\cos[\varphi_1 + 2\pi f_{\text{mod}}(N-1)\,T_{\text{p}}]. \tag{6}$$

In our experiment and numerical simulation, the modulation frequency f_{SG} was taken to be high in order to increase the PP frequency shift. By contrast, the detuning of frequency f_{SG} from multiples of the PP frequency was taken to be near a few hertz for convenience of experimental data analysis and interpretation. Most measurements were made at a constant f_{SG} of 12.001 kHz. The PP repetition rate f_{mod} was then 1 kHz. In this case, because of the stroboscopic effect, the shift of the optical carrier frequency of PPs varies slowly with time according to a harmonic law at a frequency $f_{\text{mod}} = 1$ Hz [see (6)] with an amplitude $\Delta\omega_0$ given by (3).

Changes in the spectrum of light propagating through the PZT are so small that they can only be detected using interferometric or heterodyne measurement techniques.

Figure 1 shows a schematic of the experimental setup. It comprises a ϕOTDR (delineated by a dot-dashed line in Fig. 1); a fibre line formed by two spooled pieces of fibre 1 and 79 km long, with a region of strong determinate disturbance (PZT); and a scheme for measuring variations in PP frequency and backscattered signal. In control measurements, the PZT could be located not only in the fibre line (position marked by point A) but also at points B and C. At point B, the PZT acted only on PPs, without influencing scattered light, whereas at point C it acted only on scattered light.

The acousto-optic modulator (AOM) in the ϕOTDR converted the cw laser output to PPs, which were amplified by an erbium-doped fibre amplifier (EDFA1) and sent to the fibre line. The backscattered signal travelled through a circulator to the receiver part of the reflectometer, which comprised an

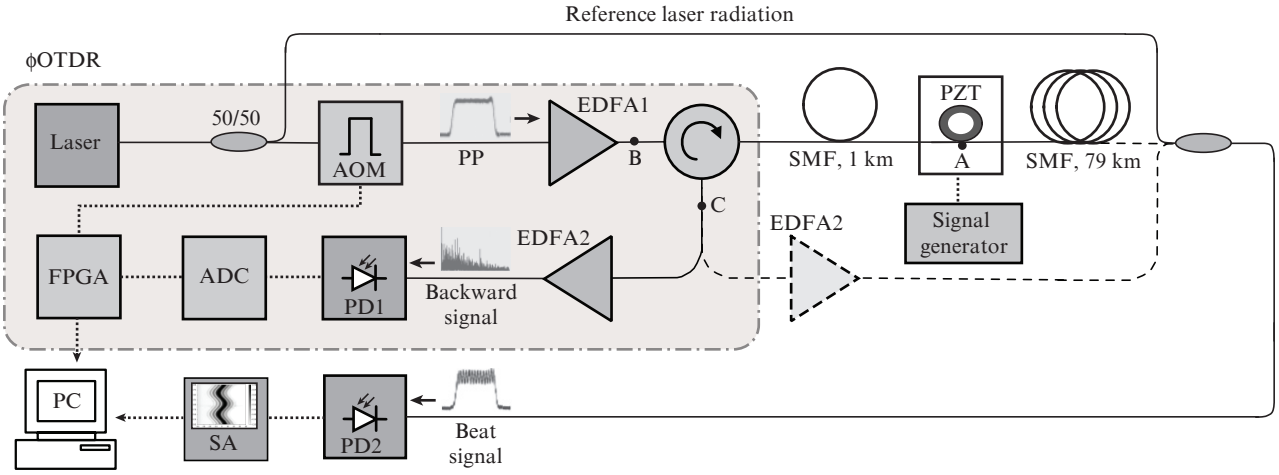

Figure 1. Schematic of the experimental setup (the PZT was placed in three positions, marked by the letters A, B, and C). The fibre with reference laser radiation was connected to the end of the line to measure the PP frequency shift and to the output of amplifier EDFA2 to measure the frequency offset in the reflectometer.

optical preamplifier (EDFA2), photodetector (PD1), analogue-to-digital converter (ADC), and field-programmable gate array (FPGA). Data from the FPGA were processed on a computer (PC). The ϕOTDR operated in two modes: amplitude (single-pulse) and phase (dual-pulse) modes. In both cases, the pulse repetition rate was f_p = 1 kHz and the pulse duration was τ_p = 200 ns. In the amplitude mode, fibre was probed by single pulses [1] and we analysed only amplitude ϕOTDR traces: time dependences of the photodetector current, proportional to the optical power (intensity): $P(t) \sim |E(t)|^2$. From amplitude ϕOTDR traces, one can determine the place of an external disturbance, but fibre elongation cannot be determined because of the nonlinearity of the response. In the phase mode, fibre was probed by a sequence of four pairs of pulses with a phase difference $\psi \in [0, \pi/2, \pi, 3\pi/2]$ and a pulse separation in each pair τ_d = 300 ns, which allowed us to restore the so-called differential phase: the phase difference between the signals resulting from the backscattering of the first and second pulses [10, 11]. From the measured differential phase, one can evaluate fibre elongation.

To study variations in the PP carrier, we used heterodyne measurements. For this purpose, a Mach–Zehnder interferometer (MZI) was added to the scheme. Through its short arm, reference light from the laser present in the ϕOTDR propagated, and the PZT-containing fibre line under study was used as the long arm of the interferometer. The beat signal at the MZI output was detected by an Alphalas UPD-15-IR2 photodetector (PD2) and R&S FSW8 signal and spectrum analyser (SA), whose output was processed on a PC.

In a similar way, we measured variations in the optical carrier frequency of backscattered light. To this end, the light from the EDFA2 output was also heterodyned with reference laser radiation.

3. Description of the numerical model for ϕOTDR operation

As a base, we used a model described by Mermelstein et al. [16], in which PPs were assumed to be quasi-monochromatic and rectangular in shape, the average density of evenly distributed Rayleigh centres (RCs) was 1 m^{-1}, the time sample spacing was dt = 1 ns, the time separation between ϕOTDR traces was $dT = f_p^{-1}$ = 1 ms, and the fibre was assumed to be one-dimensional, i.e. the RCs were randomly distributed along the fibre length. The complex-valued amplitude of a ϕOTDR trace at time t, corresponding to the longitudinal coordinate $z = v_g t/2$, can be represented as the sum of partial pulses backscattered by RCs with coordinates ξ_m in the range $L_{sc} = v_g \tau_p/2$ centred at point z (here v_g is the PP group velocity):

$$E(t) = \gamma E_0 \exp(-\alpha z)\exp(2ikn z)\frac{1}{\sqrt{M}}\sum_m^M \exp(2ikn\xi_m), \quad (7)$$

where γ is the amplitude coefficient of Rayleigh backscattering; E_0 is the PP amplitude; α is the intensity attenuation coefficient in the fibre; n is the refractive index of the fibre; $k = \omega/v_\varphi$ is the wavenumber; v_φ is the PP phase velocity in the fibre; and M is the number of RCs in the range L_{sc}. The arrangement of RCs around point z in the fibre is schematised in Fig. 2.

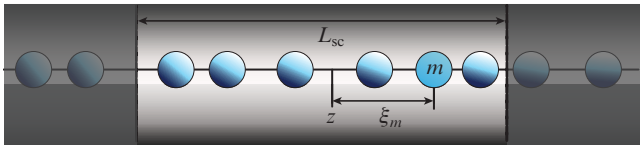

Figure 2. Arrangement of RCs in a single-mode optical fibre around point z.

The amplitude of a dual-pulse ϕOTDR trace, $R(t)_{K,l}$, where K is the number of phase measurement and l = 1–4 is the number of a ϕOTDR trace in a given measurement, can be represented as the sum of the amplitudes of single-pulse ϕOTDR traces with allowance for the corresponding shift by the delay time t_d and the additional phase $\psi_l = [0, \pi/2, \pi, 3\pi/2]$:

$$R(t)_{K,l} = |E(t) + E(t - \tau_d)\exp(i\psi_l)|^2. \quad (8)$$

The actual number of a ϕOTDR trace is $N = 4(K-1) + l$. The phase change in time t_d can be found from a sequence of four such ϕOTDR traces as the argument of a complex number:

$$\varphi(K, t) = \arg[(R(t)_{K,1} - R(t)_{K,3}) + \mathrm{i}(R(t)_{K,2} - R(t)_{K,4})]. \quad (9)$$

To simulate the PZT placed in the fibre line, Eqn (7) should include the exponential term $\exp[2\mathrm{i}\varphi_{\mathrm{mod}_m}(z_m, N)]$, which takes into account the displacement of an RC as a result of fibre elongation under the effect of the PZT, where $\varphi_{\mathrm{mod}_m}(z_m, N)$ is a function of the coordinate of the RC ($z_m = z + \xi_m$) and the number of the ϕOTDR trace (N):

$$\varphi_{\mathrm{mod}_m}(z, N) =$$

$$\begin{cases} 0, & z_m \leqslant z_{\mathrm{PZT}}, \\ \dfrac{z_m - z_{\mathrm{PZT}}}{L}\left[KU_0 \sin\left(2\pi f_{\mathrm{SG}} \dfrac{z_m n}{c}\right)\right. & \\ \left. + \Delta\omega(N)\dfrac{z_m n}{c}\right], & z_{\mathrm{PZT}} < z_m \leqslant z_{\mathrm{PZT}} + L, \\ KU_0 \sin\left[2\pi f_{\mathrm{SG}} \dfrac{(z_{\mathrm{PZT}} + L)n}{c}\right] + \Delta\omega(N)\dfrac{z_m n}{c}, & z_m > z_{\mathrm{PZT}} + L \end{cases} \quad (10)$$

(here L is the length of the fibre in the PZT and z_{PZT} is the coordinate of the closer boundary of the PZT). Equation (7), with simulation of the PZT placed in the fibre line, then takes the following form:

$$E(t)_N = \gamma E_0 \exp(-\alpha z)\exp(2\mathrm{i}knz)\frac{1}{\sqrt{M}} \times \sum_m^M \exp(2\mathrm{i}kn\xi_m)\exp[2\mathrm{i}\varphi_{\mathrm{mod}_m}(z + \xi_m, N)]. \quad (11)$$

4. Results and discussion

4.1. Effect of the PZT on the spectrum of signals

The shift of the optical carrier frequency and the spectrum of PPs were measured by the beat method: reference cw laser radiation was mixed with PPs at the output of the fibre line. The external disturbance to be studied was produced by the operating PZT modulator, located at point A or B (Fig. 1). In our experiment, the PP repetition rate, $f_{\mathrm{p}} = 1$ kHz, was lower than the PZT modulation frequency f_{SG}, so the PP carrier frequency varied with time at frequency f_{mod}, determined by the stroboscopic effect [see (6)]. From the beat signal between reference light and PPs, we obtained a spectrogram, which was used to determine the frequency shift from the shift of the peak position. Figure 3a shows the time dependence of the shift of the optical carrier frequency at $f_{\mathrm{SG}} = 12.001$ kHz and $f_{\mathrm{p}} = 1$ kHz: the PP carrier frequency envelope varies harmonically at a frequency $f_{\mathrm{mod}} = 1$ Hz, in full agreement with relation (6). At a 5-V voltage applied to the PZT, the maximum shift of the optical carrier frequency is $\Delta\nu_0 = 5.34\,(\pm 0.1)$ MHz (at a modulation frequency of 12.001 kHz). The inset in Fig. 3a shows spectra of PPs at a carrier frequency shift of 0, +5.34, and −5.34 MHz, which corresponds to a time of 0, 0.25, and 0.75 s. The absence of changes in line shape (except for the centre frequency) confirms that the effect of frequency modulation within a PP can be neglected.

In a similar way, we analysed the time dependence of the shift of the optical carrier frequency of Rayleigh backscattering under the effect of the PZT located at point C. Figure 3b demonstrates that, at a frequency $f_{\mathrm{SG}} = 12.001$ kHz, the ϕOTDR trace centre frequency also oscillates at frequency f_{SG} with an amplitude $\Delta\nu_0 = 5.34$ MHz. Thus, a strong impact on a short PP shifts its optical carrier frequency, and an impact

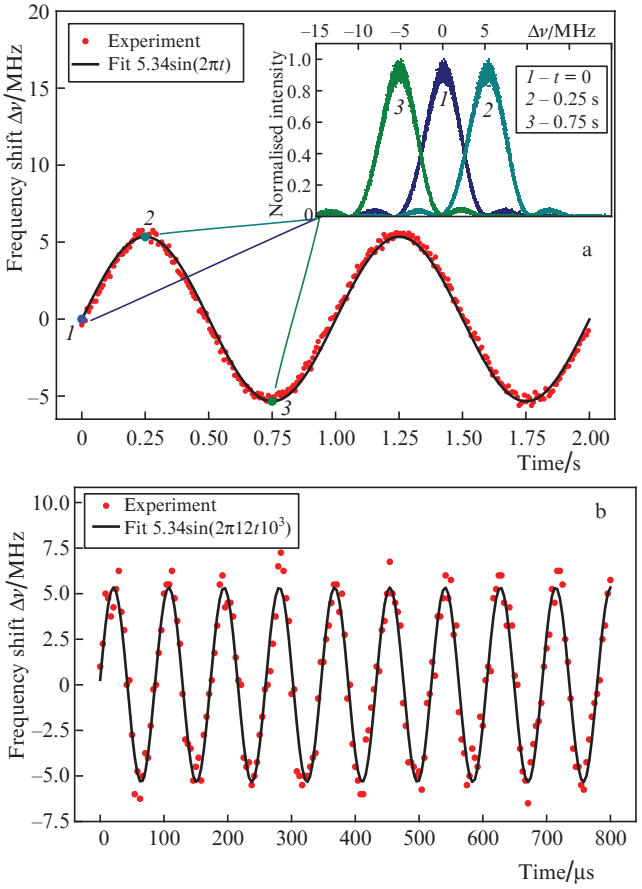

Figure 3. Optical carrier frequency shift caused by periodic elongation of the PZT section: (a) time dependence of the shift of the optical carrier frequency of PPs at $f_{\mathrm{SG}} = 12.001$ kHz and $f_{\mathrm{p}} = 1$ kHz (inset: spectra of PPs at $\Delta\nu = 0$, 5.34, and −5.34 MHz, which corresponds to 0, 0.25, and 0.75 s); (b) time dependence of the shift of the optical carrier frequency of backscattered light (the PZT is located at point C). The modulation frequency coincides with $f_{\mathrm{SG}} = 12.001$ kHz.

on the backscattered signal ($\tau_{\mathrm{p}} \geqslant f_{\mathrm{SG}}^{-1}$) leads to a time-dependent shift of the backscattered light carrier frequency. If the PZT is located at point A, there are both a shift of the PP carrier frequency and frequency modulation of scattered light. At the same time, as demonstrated by the experimental data in Section 4.2, a shift of the PP carrier frequency influences amplitude ϕOTDR traces of the fibre beyond the affected region, whereas frequency modulation of the already scattered light has no effect on the time dependence of the scattered light intensity, i.e. amplitude ϕOTDR traces remain unchanged.

4.2. Effect of the PZT on ϕOTDR operation in amplitude mode

In a phase-sensitive reflectometer, the coherence time of the source exceeds the PP duration, so partial waves scattered by the RCs located within half the spatial pulse length, L_{sc}, add up with allowance for their phases (Fig. 2). Since the RCs are arranged at random, the phases of the partial waves are random values. As a result, the observed time dependence of the scattered light intensity, referred to as an amplitude OTDR trace, has a jagged shape and is a 1D analogue of a speckle pattern. Examples of OTDR traces can be found in many reports (see e.g. Ref. [28]).

In the case of an external vibroacoustic disturbance, a coherent reflectometer records a sequence of ϕOTDR traces and variations in their shape. Figures 4a–4c show difference ϕOTDR traces, $P^*_{\Delta T}(z)$, calculated using Eqn (11) for four ΔT values: 10, 50, 100, and 200 ms. A difference OTDR trace is the difference between two OTDR traces with a time delay ΔT:

$$P^*_{\Delta T}(z) = P_{\Delta T}(z) - P_0(z). \quad (12)$$

The curves in Fig. 4 differ in modulation frequency, whereas the stretching amplitude is constant over a 30-m length (coordinates from 1110 to 1140 m). The external disturbance changes the positions of RCs in the affected region, leading to changes in ϕOTDR traces in the stretching region. Since the relative arrangement of the RCs beyond the affected region remains unchanged, in the case of a weak effect of an external disturbance on PPs ϕOTDR traces remain unchanged beyond the affected region (Fig. 4a). If an external disturbance changes the PP frequency, the entire ϕOTDR trace beyond the affected region undergoes changes, which grow with frequency shift, as illustrated by Figs 4b and 4c. In the case of distributed sensors, such changes in OTDR traces are interference because they make external influences more difficult to detect.

As follows from Fig. 4, a key parameter determining the magnitude of induced interference is the relative frequency shift $\Delta\nu\tau_p$. The maximum level of the interference induced in a ϕOTDR trace is observed at $\Delta\nu\tau_p = 1$, which corresponds to a frequency shift of 5 MHz at a pulse duration $\tau_p = 200$ ns. At a small frequency shift (of the order of 0.4 kHz), there is essentially no interference and, as seen from Fig. 4a, in this case the reflectometer detects only the local disturbance. The size of the zone where changes in the ϕOTDR trace are observed exceeds that of the region itself, because the response of the reflectometer to the PZT-induced disturbance is the convolution of the spatial pulse shape and the affected region, multiplied by a random response function.

Increasing the amplitude of the shift of the PP carrier frequency produces interference behind the affected region. Thus, numerical simulation results confirm that the experimentally observed interference to the reflectometer signal behind the strong local disturbance region can be accounted for by the shift of the optical carrier frequency of PPs (Fig. 2a). In contrast, the frequency shift of the already scattered light as a result of propagation through the PZT in the backward direction (Fig. 2b) has no effect on the shape of the ϕOTDR trace, nor does it produce interference. Note that, in numerical simulation, the function representing the frequency modulation of scattered light was turned on and off, but the shape of the ϕOTDR trace remained unchanged.

To gain direct experimental evidence that the frequency modulation of the already scattered light had no effect on the shape of the ϕOTDR trace, the PZT was placed at point B or C. If the modulator was placed at point B, interference emerged throughout the ϕOTDR trace, even though there was no modulation of the scattered light. By contrast, placing the PZT at point C resulted in scattered light modulation, but no changes in the shape of ϕOTDR traces were detected because in this case there was no modulation of the optical carrier frequency of PPs.

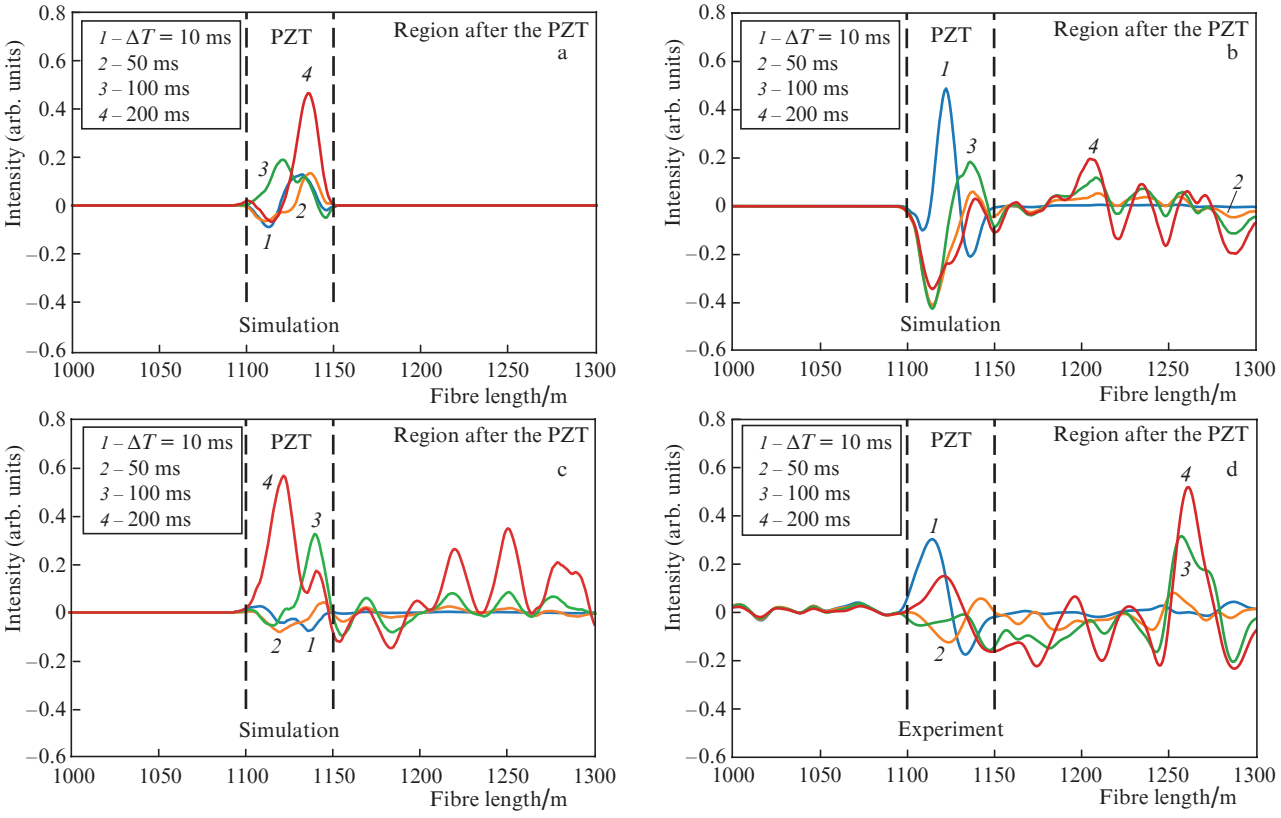

Figure 4. Difference ϕOTDR traces at modulation frequencies of (a) 1, (b) 6001, and (c, d) 12 001 Hz. The corresponding maximum frequency shift is $\Delta\nu = (d\varphi_{mod}/dt)/2\pi = 0.0004$, 2.67, and 5.34 MHz. The stretching amplitude ΔL in the range 1110–1140 m is constant at 2.6 μm m^{-1} ($\varphi_{mod} = 140\pi$). The PZT signal was observed at lengths from 1100 to 1150 m due to the contribution of the ϕOTDR resolution (20 m).

For constant monitoring of external influences on the sensing element of a distributed sensor, one should constantly analyse difference OTDR traces. Such analysis was carried out by us both in automatic mode, with the use of application software, and visually. For visual analysis, sequences of difference ϕOTDR traces were displayed on a monitor in real time, so that we obtained a 3D graph of power variations against time and coordinate along the distributed sensor. Due to the constant updating of OTDR traces, the observed picture constantly moved on the display. Hereafter, such 'moving' 3D graphs will be referred to as spatiotemporal diagrams (STDs).

Figure 5 shows STDs of power variations obtained for a ϕOTDR by numerical simulation and experimentally under conditions similar to those of obtaining difference ϕOTDR traces (Fig. 4). In all cases, the PZT was located at point A and an external disturbance was produced in the fibre section with coordinates from 1110 to 1140 m. The maximum frequency change was 5.34 MHz.

In the calculated STDs, the elongation is constant in sequential ϕOTDR traces, whereas the shift of the optical carrier of PPs rises systematically. In Fig. 5a, the PP frequency shift is small (0.4 kHz) and the interference is essentially indiscernible. As clearly demonstrated in Figs 5b and 5c, increasing the maximum frequency shift (2.67 and 5.34 MHz) gives rise to interference behind the PZT region: after the point with a coordinate of 1150 m [like in individual ϕOTDR traces (Fig. 4), the response to the PZT in the STDs is the convolution of the spatial pulse shape and the affected region, multiplied by a random response function]. The experimentally obtained STD in Fig. 5d agrees well with the calculated one in Fig. 5c.

Thus, the present results show that a strong and rapidly varying elongation modulation in some finite fibre section (region of a strong local disturbance) produces interference in the portion of the ϕOTDR trace behind the affected region. The assumed mechanism of interference due to a strong local disturbance is the shift of the probe pulse frequency, so the degree of distortion of the ϕOTDR trace is determined by the time derivative of the phase shift, $d\varphi_{mod}/dt$ (rad s^{-1}), which is equal to the shift of the angular frequency of probe pulses, $\Delta\omega$ (rad s^{-1}). It is convenient to convert this quantity to the frequency shift $\Delta\nu$ (Hz): $\Delta\nu = \Delta\omega/2\pi$.

The interference induced in the region located behind the local disturbance zone can be quantified using Pearson correlation: If the correlation coefficient is near unity, the local disturbance has a relatively weak effect on the reflectometer signal beyond the affected region. If the correlation coefficient is near zero, beyond the affected region the reflectometer records a false signal (interference) with a maximum amplitude, which prevents its normal operation. However, even substantially weaker distortions of the ϕOTDR trace, caused by the PP frequency shift due to a local disturbance, limit reflectometer sensitivity. Indeed, since ϕOTDR sensitiv-

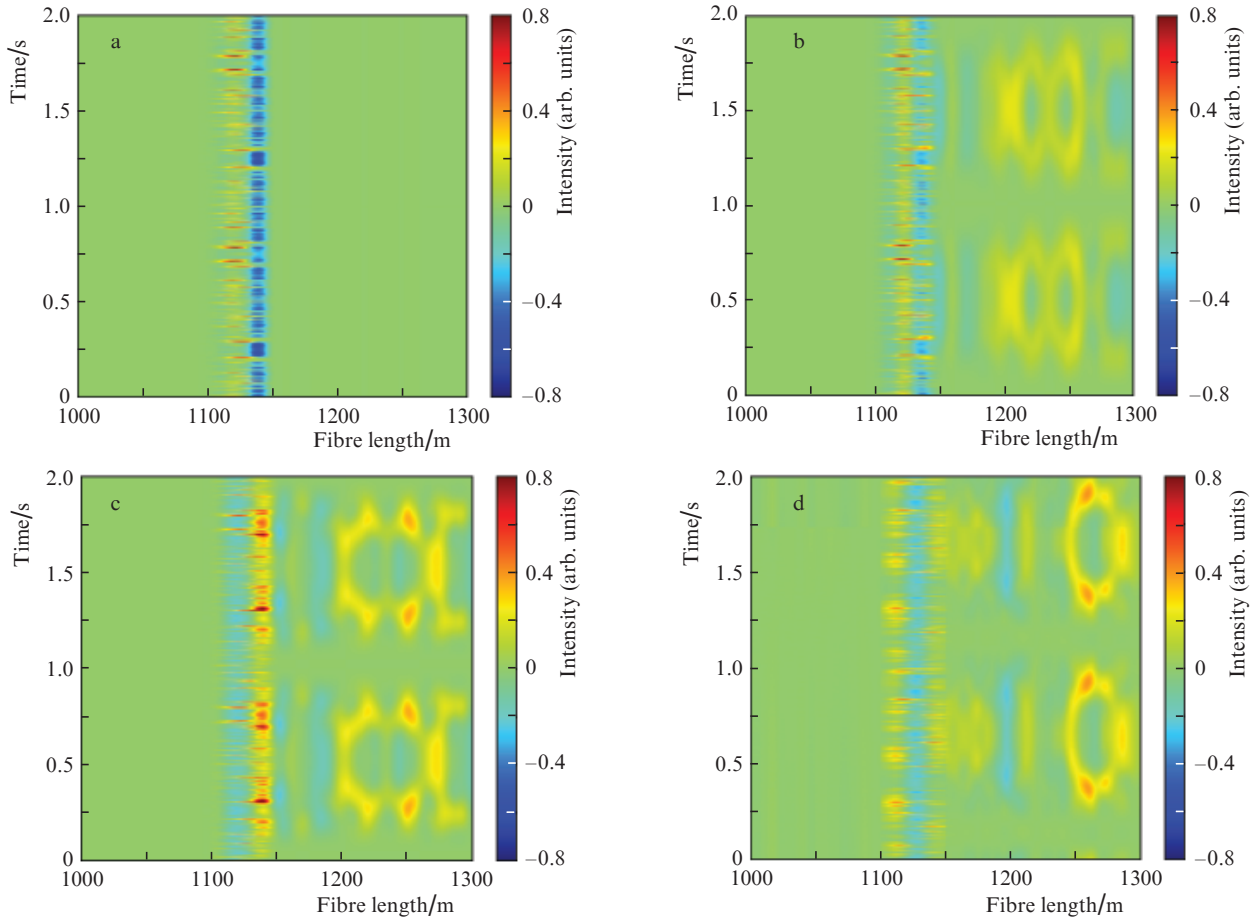

Figure 5. (Colour online) Spatiotemporal diagrams obtained for difference ϕOTDR traces by (a–c) numerical simulation and (d) experimentally at modulation frequencies of (a) 1, (b) 6001, and (c, d) 12 001 Hz. The corresponding maximum frequency shift is $(d\varphi_{mod}/dt)/2\pi$ = 0.0004, 2.67, and 5.34 MHz.

ity at a large signal-to-noise ratio is limited by the emission bandwidth $\Delta\nu_{las}$ of the cw master oscillator, detectable interference emerges if the constraint $d\varphi_{mod}/dt > 2\pi\Delta\nu_{las}$ is fulfilled, which can be thought of as a strong influence condition. Since the bandwidth of master oscillators in state-of-the-art ϕOTDR is a few kilohertz, at an external disturbance frequency of the order of 10 kHz the influence is strong even at a phase shift modulation amplitude as small as a few radians.

According to Mermelstein et al. [16], the Pearson correlation coefficient is given by

$$C_{i,j} = \frac{\langle \Delta I_i \Delta I_j \rangle}{\sqrt{\langle \Delta I_i \rangle^2 \langle \Delta I_j \rangle^2}}, \tag{13}$$

where $\Delta I = I - \langle I \rangle$; I is intensity; and i and j are the ϕOTDR trace numbers. Figure 6 shows experimentally determined and simulated Pearson correlation coefficients between pairs of ϕOTDR traces against the difference between the optical carrier frequencies of PPs in the ϕOTDR traces being compared.

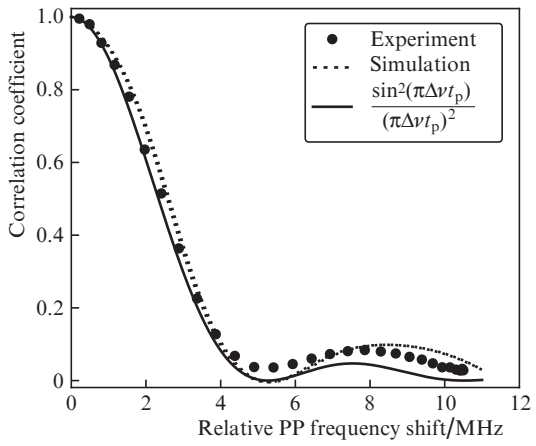

Figure 6. Pearson correlation coefficient as a function of the relative difference between the PP frequencies in ϕOTDR traces being compared: the solid circles are the experimental data, the dotted line represents the numerical simulation results, and the solid line represents the corresponding analytical relation [16].

In our experiment, the PP frequency shift relative to the cw laser frequency was varied from –5.34 to +5.34 MHz. We examined Pearson correlation between ϕOTDR traces of PPs with a frequency shift of –5.34 MHz and other ϕOTDR traces with frequency shifts in the above range (accordingly, the PP frequency difference varied in the range 0–10.7 MHz). The correlation coefficient was calculated over a 5-km length, with the PZT located at point B.

The dependences of the Pearson correlation coefficient on the difference between optical PP frequencies obtained by processing the experimental and numerically calculated ϕOTDR traces are essentially identical to each other and to the theoretical analytical dependence $C(\Delta\nu) = \mathrm{sinc}^2(\pi\Delta\nu t_p)$ derived by Mermelstein et al. [16] for small frequency differences. The poorer agreement between the curves at frequencies of the order of and above the complete decorrelation frequency (5 MHz) can be accounted for by the lower calculation accuracy in the case of near-zero correlations.

Thus, the present experimental data and numerical simulation results confirm that the change in PP centre frequency as a result of an external influence on the fibre produces interference behind the affected region. In contrast, variations in the optical carrier frequency of an already existing Rayleigh backscattering wave have no effect on single-pulse ϕOTDR operation. The reason for this is that optical carrier frequency (phase) modulation on its own causes no changes in the amplitude or intensity of the wave and, accordingly, does not change those of the measured amplitude ϕOTDR trace.

4.3. Effect of the PZT on ϕOTDR operation in phase mode

As pointed out in many reports, one drawback to amplitude ϕOTDRs is that the response of the distributed sensor to an external influence is nonlinear. Such a reflectometer allows one to locate the place of a disturbance, but it cannot be used for quantitative measurements. Fibre elongation due to external influences can be quantitatively measured with a ϕOTDR operating in phase mode, e.g. using a dual-pulse phase ϕOTDR [2, 10, 11]. In a phase ϕOTDR, analysis of a sequence of four ϕOTDR traces allows one to calculate the phase difference between the wave resulting from scattering of the first pulse and the wave resulting from scattering of the second pulse. The coordinate dependence of the differential phase (or restored phase) obtained by point-by-point processing of four ϕOTDR traces will be referred to as a phase ϕOTDR trace. Like an amplitude ϕOTDR trace, a phase ϕOTDR trace is a random function of coordinate and carries no information about the external influence.

In an experimental study of the effect of strong local disturbances on the operation of a dual-pulse phase ϕOTDR, we recorded variations in phase ϕOTDR traces using difference differential ϕOTDR traces. Differential ϕOTDR traces show the phase difference between waves scattered by the first and second pulses in a pair:

$$\Phi(t) = \phi(t) - \phi(t - \tau_d). \tag{14}$$

The most informative – and the most convenient for visual analysis – method of detecting changes in phase ϕOTDR traces is to display on a monitor in real time a sequence of difference differential phase ϕOTDR traces, i.e. differences between differential phase ϕOTDR traces with a time delay ΔT:

$$\Phi^*_{\Delta T}(z) = \Phi_{\Delta T}(z) - \Phi_0(z). \tag{15}$$

As a result, we obtain a 3D graph of the differential phase difference against time and coordinate along the distributed sensor. Due to the constant updating of ϕOTDR traces, the observed picture constantly moves on the display, like in the case of STDs. Hereafter, by analogy with STDs, such 'moving' 3D graphs will be referred to as spatiotemporal differential phase diagrams (STDPDs).

Figure 7 shows STDPDs obtained for a phase ϕOTDR by numerical simulation and experimentally. They have the form of a vertical time sweep of many sequential 1D horizontal difference differential phase ϕOTDR traces. The horizontal position of points in these ϕOTDR traces corresponds to their coordinate, and their colour corresponds to the change in the phase difference between backscattered waves of two pulses. Due to the strong influence of the PZT, the ϕOTDR signal in the STDPDs in the PZT region inadequately represents the phase shift, because the amplitude of the disturbance exceeds

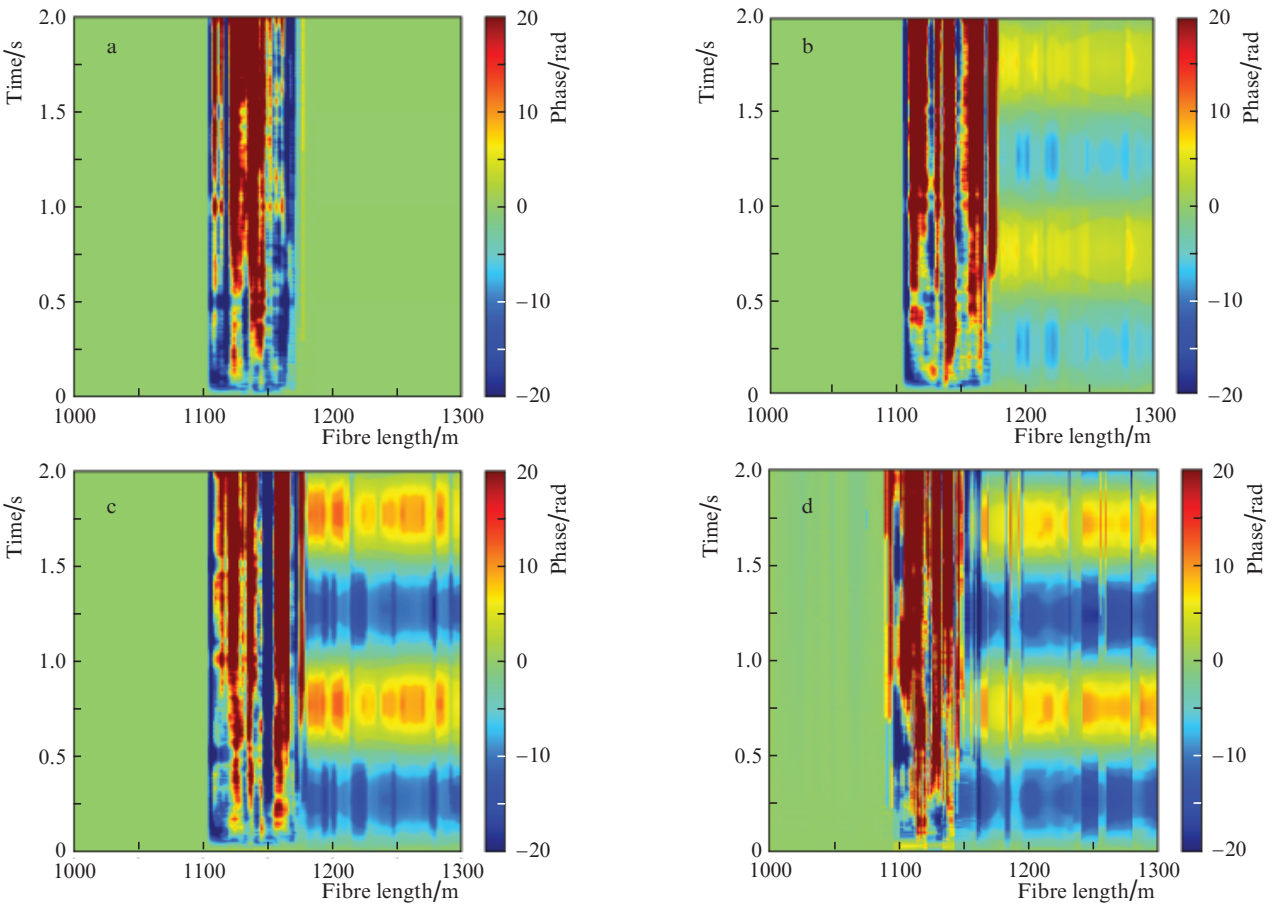

Figure 7. (Colour online) STDPDs of a phase ϕOTDR for a local periodic stretching of a 30-m length of fibre (between 1110 and 1140 m) with the PZT, obtained (a–c) as a result of numerical simulation and (d) experimentally at identical stretching amplitudes and modulation frequencies of (a) 1, (b) 6001, and (c, d) 12 001 Hz. The corresponding maximum frequency shift is $\Delta\nu = (d\varphi_{mod}/dt)/2\pi = 0.0004$, 2.67, and 5.34 MHz.

the dynamic range of a linear variation in the differential phase.

The present results demonstrate that the change in PP centre frequency in the strong disturbance region produces interference in phase ϕOTDR traces behind the affected region as a result of changes in the phase of partial waves scattered by random inhomogeneities and unrelated to the actual disturbance of the fibre in this region. In the case of a strong sinusoidal disturbance, distortions show up as false signals that emerge in the STDPD behind the strong disturbance region and have the form of horizontally elongated structures. Like in the case of a single-pulse amplitude ϕOTDR, backscattered light frequency modulation in the strong disturbance region has no effect on the operation of a dual-pulse phase ϕOTDR because the phase is evaluated from measured intensities in ϕOTDR traces, which remain unchanged in the case of phase modulation of scattered light. This conclusion was verified and supported by experimental data with the PZT at point C: turning the PZT on and off had no effect on the shape of phase ϕOTDR signals.

5. Conclusions

Distortions of a ϕOTDR trace in fibre behind a strong local disturbance region have for the first time been detected experimentally and confirmed by numerical simulation. The distortions show up as interference (false signal) that impedes ϕOTDR detection of weak disturbances throughout the fibre behind the local disturbance region. The interference mechanism has been shown to be related to changes in ϕOTDR trace intensity due to the shift of the optical frequency of probe pulses in the strong local disturbance region. Since the optical frequency shift due to the strong local disturbance is proportional to the rate of changes in phase shift, at a constant local disturbance amplitude the shift increases with disturbance frequency, which can in general far exceed the probe pulse frequency.

The distortion of the reflectometer signal behind the local disturbance region can be quantified by numerically calculating the Pearson correlation coefficient for the intensity of ϕOTDR traces, which is unity in an ideal case (the ϕOTDR trace intensity does not vary from pulse to pulse) and decreases in the presence of interference. Under the present experimental conditions, at a probe pulse duration of 200 ns, the Pearson correlation coefficient drops to zero at a probe pulse frequency shift $\Delta\nu$ = 5 kHz. Clearly, under actual ϕOTDR application conditions such strong external influences are encountered very rarely. Nevertheless, even considerably weaker local disturbances which cause a three order of magnitude smaller frequency shift (a few kilohertz) may reduce the sensitivity of the distributed sensor behind the local disturbance region.

The present experimental data and numerical simulation results demonstrate that, in the case of a strong local disturbance, interference behind the disturbance region emerges in phase mode of ϕOTDR operation as well. In such a case, phase ϕOTDR traces show false differential phase shifts,

which are well seen in spatiotemporal differential phase diagrams (Fig. 7).

The present results are of practical importance because ϕOTDRs are employed in areas where extremely high sensitivity is needed to detect and record weak disturbances [29–33]. The possibility of interference from relatively strong local disturbances capable of impeding detection of the signal from a weak disturbance should be taken into account e.g. in using a ϕOTDR for monitoring the state of railways, where it is necessary to detect and record a weak signal from a walking man in the presence of very strong disturbances produced by moving trains [29, 32]. This effect should also be taken into account when using other phase-sensitive fibre-optic sensors.

References

1. Shatalin S.V., Treschikov V.N., Rogers A.J. *Appl. Opt.*, **37** (24), 5600 (1998).
2. Lukashova T.O. et al. *Quantum Electron.*, **50** (9), 882 (2020) [*Kvantovaya Elektron.*, **50** (9), 882 (2020)].
3. Peng F. et al. *IEEE Photonics Technol. Lett.*, **26** (20), 2055 (2014).
4. Nesterov E.T., Treshchikov V.N., Ozerov A.Zh., Sleptsov M.A., Kamynin V.A., Nanii O.E., Sus'yan A.A. *Tech. Phys. Lett.*, **37** (5), 417 (2011) [*Pis'ma Zh. Tekh. Fiz.*, **37** (9), 55 (2011)].
5. Liu T., Wang F., Zhang X., Zhang L., Yuan Q., Liu Y., Yan Z. *Opt. Eng.*, **56**, 084104 (2017).
6. Wang C., Shang Y., Liu X.-H., Wang C., Yu H.-H., Jiang D.-S., Peng G.-D. *Opt. Express*, **23**, 29038 (2015).
7. Kharasov D.R., Bengalskii D.M., Vyatkin M.Yu., Nanii O.E., Fomiryakov E.A., Nikitin S.P., Popov S.M., Chamorovsky Yu.K., Treshchikov V.N. *Quantum Electron.*, **50** (5), 510 (2020) [*Kvantovaya Elektron.*, **50** (5), 510 (2020)].
8. Zhu F., Zhang Y., Xia L., Wu X., Zhang X. *J. Lightwave Technol.*, **33**, 4775 (2015).
9. Hicke K., Eisermann R., Chruscicki S. *Sensors*, **19** (19), 4114 (2019).
10. Nikitin S.P. et al. *Laser Phys.*, **28** (8), 085107 (2018).
11. Treshchikov V.N. et al. RF Patent No. 2 562 689 (2014).
12. Alekseev A.E. et al. *Laser Phys.*, **24** (11), 115106 (2014).
13. Posey R., Johnson G.A., Vohra S.T. *Electron. Lett.*, **36** (20), 1688 (2000).
14. Kirkendall C.K., Dandridge A. *J. Phys. D: Appl. Phys.*, **37** (18), R197 (2004).
15. Nikitin S. et al. *J. Lightwave Technol.*, **38** (6), 1446 (2020).
16. Mermelstein M.D., Posey R., Johnson G.A., Vohra S.T. *Opt. Lett.*, **26** (2), 58 (2001).
17. Zhirnov A.A. et al. *Opt. Spektrosk.*, **127** (10), 603 (2019).
18. Zhu F. et al. *IEEE Photonics Technol. Lett.*, **27** (24), 2523 (2015).
19. Nikitin S.P., Ulanovskiy P.I., Kuzmenkov A.I., Nanii O.E., Treshchikov V.N. *Laser Phys.*, **26** (10), 105106 (2016).
20. Nesterov E.T. et al. *J. Phys.: Conf. Ser.*, **584** (1), 012028 (2015).
21. Martins H.F. et al. *Opt. Lett.*, **38** (6), 872 (2013).
22. Kharasov D.R. et al. *Trudy 8-go Rossiiskogo seminara po volokonnym lazeram* (Proc. 6th Russian Workshop on Fibre Lasers) (Novosibirsk, 2018) pp. 208–210.
23. Martins H.F. et al. *J. Lightwave Technol.*, **32** (8), 1510 (2014).
24. Kharasov D.R. et al. *Proc. Int. Conf. Laser Optics* (ICLO) 2018 (St. Petersburg, 2018) p. 285.
25. Wang Z.N. et al. *Opt. Lett.*, **39** (15), 4313 (2014).
26. Alekseev A.E., Gorshkov B.G., Potapov V.T. *Laser Phys.*, **29** (5), 055106 (2019).
27. Alekseev A.E. et al. *Laser Phys.*, **30** (3), 035107 (2020).
28. Gorshkov B.G. et al. *Quantum Electron.*, **36** (10), 963 (2006) [*Kvantovaya Elektron.*, **36** (10), 963 (2006)].
29. Nan Q. et al. *Sensors*, **19** (12), 2666 (2019).
30. Daley T.M., Freifeld B.M., Ajo-Franklin J., Dou S., Pevzner R., Shulakova V., Kashikar S., Miller E.D., Goetz J., Henninges J., Lueth S. *Leading Edge*, **32** (6), 699 (2013).
31. Peng F., Duan N., Rao Y.-J., Li J. *IEEE Photonics Technol. Lett.*, **26** (20), 2055 (2014).
32. Li Z. et al. *Opt. Express*, **28** (3), 2925 (2020).
33. Wu H., Wang Z., Peng F., Peng Z., Li X., Wu Y., Rao Y. *Proc. SPIE*, **9157**, 915790 (2014).